01 Jan 2015

Electron- and Photon-Impact Ionization of Furfural

D. B. Jones

E. Ali

K. L. Nixon

P. Limão-Vieira

et. al. For a complete list of authors, see https://scholarsmine.mst.edu/phys_facwork/453

Recommended Citation

D. B. Jones and E. Ali and K. L. Nixon and P. Limão-Vieira and M. Hubin-Franskin and J. Delwiche and C. G. Ning and J. Colgan and A. J. Murray and D. H. Madison and M. .. Brunger, "Electron- and Photon-Impact Ionization of Furfural," *Journal of Chemical Physics*, vol. 143, no. 18, American Institute of Physics (AIP), Jan 2015.
The definitive version is available at https://doi.org/10.1063/1.4935444

Electron- and photon-impact ionization of furfural

D. B. Jones,[1] E. Ali,[2] K. L. Nixon,[3,4] P. Limão-Vieira,[5,a)] M.-J. Hubin-Franskin,[6] J. Delwiche,[6] C. G. Ning,[7] J. Colgan,[8] A. J. Murray,[9] D. H. Madison,[2,a)] and M. J. Brunger[1,10,a)]
[1]*School of Chemical and Physical Sciences, Flinders University, GPO Box 2100, Adelaide, SA 5001, Australia*
[2]*Department of Physics, Missouri University of Science and Technology, Rolla, Missouri 65409, USA*
[3]*Departamento de Física, Universidade Federal de Juiz de Fora, Juiz de Fora, MG, Brazil*
[4]*School of Biology, Chemistry and Forensic Science, University of Wolverhampton, Wolverhampton WV1 1LY, United Kingdom*
[5]*Laboratório de Colisões Atómicas e Moleculares, CEFITEC, Departamento de Física, Faculdade de Ciências e Tecnologia, Universidade Nova de Lisboa, 2829-516 Caparica, Portugal*
[6]*Département de Chimie, Université de Liège, Institut de Chimie-Bât. B6C, B-4000 Liège 1, Belgium*
[7]*State Key Laboratory of Low-Dimensional Quantum Physics, Department of Physics, Tsinghua University, Beijing 100084, China*
[8]*Theoretical Division, Los Alamos National Laboratory, Los Alamos, New Mexico 87545, USA*
[9]*Photon Science Institute, School of Physics and Astronomy, University of Manchester, Manchester M13 9PL, United Kingdom*
[10]*Institute of Mathematical Sciences, University of Malaya, 50603 Kuala Lumpur, Malaysia*

(Received 24 August 2015; accepted 29 October 2015; published online 12 November 2015)

The He(I) photoelectron spectrum of furfural has been investigated, with its vibrational structure assigned for the first time. The ground and excited ionized states are assigned through *ab initio* calculations performed at the outer-valence Green's function level. Triple differential cross sections (TDCSs) for electron-impact ionization of the unresolved combination of the $4a'' + 21a'$ highest and next-highest occupied molecular orbitals have also been obtained. Experimental TDCSs are recorded in a combination of asymmetric coplanar and doubly symmetric coplanar kinematics. The experimental TDCSs are compared to theoretical calculations, obtained within a molecular 3-body distorted wave framework that employed either an orientation average or proper TDCS average. The proper average calculations suggest that they may resolve some of the discrepancies regarding the angular distributions of the TDCS, when compared to calculations employing the orbital average. © *2015 AIP Publishing LLC.* [http://dx.doi.org/10.1063/1.4935444]

I. INTRODUCTION

Furfural or 2-furaldehyde ($C_5H_4O_2$) is an important chemical in the petroleum, plastics, agro-chemical, and pharmaceutical industries.[1] It has also been identified as a key platform chemical[2,3] in the commercial realisation of bio-refineries.[4] At this stage, no direct synthetic methods for furfural production exist, and it is solely produced on the industrial scale through the thermochemical treatment of biomass.[1] Hybrid interdisciplinary strategies are currently being investigated to optimize and control the chemical conversion of biomass into desirable chemicals. These include utilizing atmospheric plasma pretreatments,[5,6] or electron-beam irradiation[7,8] to overcome the natural recalcitrance of biomass. A knowledge of electron- and photon-driven processes with key bio-refinery compounds will also play an important role in understanding the chemical kinetics associated with non-thermal plasma-assisted combustion of complex biofuel-air mixtures, where conventional high-temperature combustion models may not be applicable.[9] A detailed understanding of the quantum chemical structure of the biomass sub-unit furfural, and its reaction dynamics, is therefore an important part of developing innovative techniques that can improve the energy and conversion efficiency for the processing and for the realisation of next-generation biofuels.

To partially address these requirements, an investigation into the photon- and electron-impact ionization of furfural is reported in this manuscript. Furfural is a planar molecule that can exist in either a *trans*- or *cis*-conformation (see Fig. 1). The preferred furfural structure and its rotational barrier have been the subject of many investigations (see Refs. 10 and 11 and references therein), so that it is now well established that in the gas phase the *trans* conformer is preferred, and that the relative conformation populations are *trans* (79.5%) and *cis* (20.5%). For the ionization dynamics of furfural, to the best of our knowledge there has only been one low-resolution photoelectron study undertaken.[12] A high-resolution photoionization study has therefore been carried out here, in order to characterise the vibrational structure of its low-lying ionic states. This study complements allied investigations into the electron- and photon-impact discrete excitation of furfural.[13] The dynamics of photon- and electron-impact ionization of complex polyatomic species also furthers understanding about the influence of target structure in the dynamics of the ionization process. In this respect, the triple-differential cross sections (TDCSs) for the electron-impact ionization reaction have been measured,

a)Authors to whom correspondence should be addressed. Electronic addresses: plimaovieira@fct.unl.pt; madison@mst.edu; and michael.brunger@flinders.edu.au

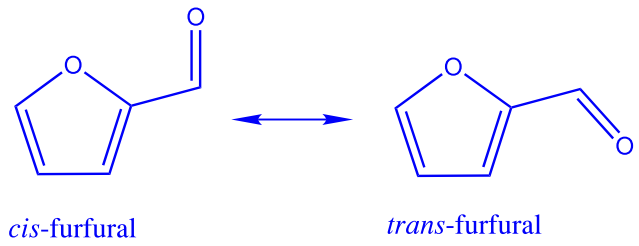

FIG. 1. Schematic representation of furfural in its *cis*- and *trans*-conformations.

$$e_0^-(E_0,\mathbf{k}_0) + M \rightarrow M^+(\epsilon,\mathbf{q}) + e_1^-(E_1,\mathbf{k}_1) + e_2^-(E_2,\mathbf{k}_2)\,. \quad (1)$$

Here, an incident electron with energy E_0 and momentum $\mathbf{k}_0$, $e_0^-(E_0,\mathbf{k}_0)$, ionizes the furfural target M (assumed to be at rest) with an ionization energy ϵ, to produce a furfural ion M^+ recoiling with a momentum $\mathbf{q}$ to conserve momentum. The energies (E_i's) and momenta ($\mathbf{k}_i$'s) of both outgoing electrons ($i = 1$ or 2) are then determined so as to observe a kinematically complete reaction. This study of furfural is performed here with a combination of asymmetric coplanar and doubly symmetric coplanar scattering geometries, as depicted in Fig. 2.

This combination of experiments, performed over a range of scattering kinematics, provides a strong test of theoretical calculations aimed at describing the electron-impact ionization process. Here, we have performed calculations at the molecular three body distorted wave (M3DW) level, that either employ an orbital average or a proper TDCS average to account for the random orientation of the molecules in the experimental studies.[14] In this way, the validity and limitation of approximations made in calculating electron scattering cross sections across a range of scattering regimes can be assessed. This also builds on earlier studies evaluating the role of molecular structure in electron-impact ionization scattering dynamics from key organic compounds.[15–20]

The outline of this manuscript is as follows. In Section II, details of the experimental configurations are presented, while in Section III, the scattering and quantum chemistry calculations are outlined. The experimental and theoretical results are then presented and discussed in Section IV. Finally, conclusions from this work are drawn in Section V.

II. EXPERIMENTAL DETAILS

A. Furfural sample

In all of the experiments described here, vapour from a liquid furfural sample (Sigma Aldrich; 99% assay) was used.

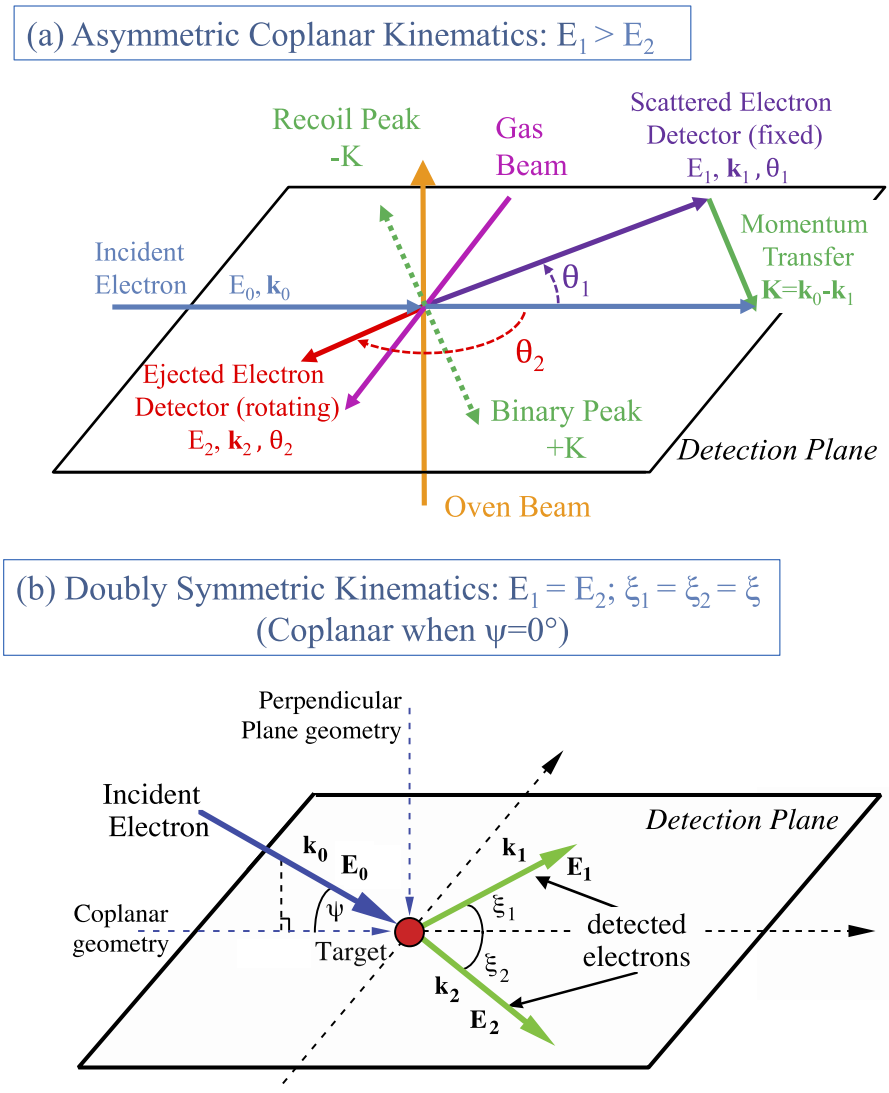

FIG. 2. Schematic diagrams of the present electron impact ionization scattering geometries. (a) The asymmetric coplanar geometry. (b) The doubly symmetric geometry, which becomes coplanar ($\psi = 0°$) when all three electrons are confined to the detection plane. The analyser angles (ξ_1 and ξ_2) are measured with respect to the projection of the incident electron beam $\mathbf{k}_0$ onto this plane as shown. See text for further details.

The samples were employed without further purification, except that they were subjected to repeated freeze pump-thaw cycles to remove dissolved gases.

B. Photoelectron experimental details

He(I) (21.22 eV) photoelectron spectra of furfural were recorded at the Université de Liège, Belgium. The apparatus that was employed has been described in detail previously.[21] Briefly, the spectrometer consists of a 180° cylindrical electrostatic analyser with a mean radius of 5 cm. The analyser is used in constant energy pass mode. The incident photons are produced by a DC discharge in a two stage differentially pumped lamp. The energy scale was calibrated using the well-known xenon lines ($^2P_{3/2}$ = 12.130 eV and $^2P_{1/2}$ = 13.435 eV).[22,23] The resolution of the present spectrum is 30 meV as determined from the full width half maximum (FWHM) of the Xe peaks in the presence of furfural. The intensities in the spectrum were corrected for the transmission of the analysing system. The accuracy of the energy scale is estimated to be ±2 meV.

C. Asymmetric coplanar kinematics experimental configuration at Flinders

TDCS for the electron impact ionization of the unresolved combination of the highest occupied and next-highest occupied molecular orbitals of furfural (HOMO+NHOMO; 4a″ + 21a′) has been measured on an apparatus housed at Flinders University. This apparatus has been described previously,[24] so only those details relating to the present measurements are repeated here. These measurements were performed in an asymmetric coplanar geometry, as depicted in Fig. 2(a). Here, an incident electron beam, with energy E_0 = 250 eV, was crossed with a beam of furfural vapour. A coincidence technique[25] was employed to measure the angular distributions of the slow ejected electron, with energy E_2 = 20 eV, while detecting the fast scattered electron at fixed scattering angles of either $\theta_1 = -5°$, $-10°$, or $-15°$. Note that the scattered electron energy was selected to conserve energy in the ionization of the unresolved HOMO+NHOMO (IP ∼9.2 eV). Here, the coincidence energy resolution was typically ∼1.1 eV (FWHM). The angular distributions for fixed scattering angles were then inter-normalised, by measuring the angular distribution of the scattered electron when the ejected electron angle is fixed at $\theta_2 = 90°$. In this way, theoretical TDCSs can be compared to the measured experimental data through a single normalisation factor applied to all experimental data. This normalisation factor was determined using a least squares technique applied to the experimental data in the binary region of the $\theta_1 = -10°$ angular distribution.

In the asymmetric coplanar geometry, the detection energy and angle of the fast scattered electron define the momentum transferred to the target ($\mathbf{K} = \mathbf{k}_0 - \mathbf{k}_1$) during the ionization process. When the slow electron leaves the collision in the direction close to that of the momentum transfer, this is considered as a binary interaction with the target. Conversely, when the slow electron is ejected in directions close to being anti-parallel to the momentum transfer direction, the residual ion must recoil with substantial momentum. These angular regions of the TDCS are then described either as the binary or recoil regions, depending on if they lie close to parallel or anti-parallel to the momentum transfer direction, respectively.

D. Doubly symmetric coplanar kinematics experimental configuration at Manchester

The experimental data collected at the University of Manchester utilised a computer controlled and computer optimised $(e,2e)$ spectrometer. This spectrometer has been described elsewhere,[26] however, the relevant details are briefly given here for completeness. The incident electron beam is produced by a two-stage electron gun. The outgoing electron analyzers are mounted on individual turntables that enable them to rotate independently around the detection plane. For this study, the spectrometer was operated in a coplanar geometry [see Fig. 2(b)], where the momentum of the incident electron $\mathbf{k}_0$ lies in the detection plane defined by the two outgoing electrons $\mathbf{k}_1$ and $\mathbf{k}_2$. Doubly symmetric kinematics were adopted with $E_1 = E_2 = E$ and $\xi_1 = \xi_2 = \xi$. In this case, E = 20 eV and ξ were scanned over the range from 35° to 120°. To ensure the spectrometer remained optimised over the time of data collection, the electrostatic lenses in the apparatus were adjusted under computer control at each angle of ξ, to maximise the electron count rate in each analyser. This corrected for any variation in the signal as the analysers swept back and forth around the detection plane. The typical coincidence energy resolution for this apparatus was determined to be ∼1.4 eV (FWHM) from the measurement of the binding energy spectrum of helium.

As furfural is a liquid at room temperature, it was necessary at both Flinders and Manchester to heat the sample and the gas handling lines to obtain sufficient target density for the measurements. In addition to this, the vacuum chamber at Manchester was also heated to ∼40 °C. High purity furfural was admitted at Manchester into the interaction region via a gas jet. The flow of furfural was regulated by a needle valve so that the vacuum in the chamber was raised from a base pressure of $\sim 1 \times 10^{-7}$ Torr to a stable working pressure of $\sim 7 \times 10^{-6}$ Torr. As a large background was observed in the coincidence timing spectrum, it was necessary to use a low incident electron beam current of ∼150 nA to improve the coincidence signal to background ratio.

The incident electron energy of the spectrometer was calibrated by measuring the coincidence binding energy spectrum of the outer valence orbitals of furfural. The incident electron energy was then set to match the energy of the structure corresponding to the unresolved HOMO and NHOMO states within the binding energy spectrum.

The data presented here for a coplanar geometry have been normalised to unity at $\xi = 45°$, since absolute measurements of the TDCS were not obtained. The theoretical calculations, obtained within different frameworks, are also normalised to unity in the region of $\xi = 45°$ to enable a comparison with the data. The uncertainty in the measurements at each angle ξ was generated from the standard error, determined from averaging the data at a given angle for all sweeps of the detection plane. Six sweeps were used to produce the TDCS,

with data being accumulated at each angle for 2000 s each sweep. The angular uncertainties in the measurements were estimated to be approximately ±3°.

III. COMPUTATIONAL METHODS

To assist in the assignment of the present spectra, quantum chemical calculations have been performed at the outer valence Green's function (OVGF)[27] level using an augmented correlation consistent valence double zeta basis set (aug-cc-pVDZ).[28,29] The ionized orbital characters were also studied using a density functional theory framework employing the B3LYP functional[30] with the same aug-cc-pVDZ basis. Here, we calculated spherically averaged orbital momentum profiles for the ionized orbitals that were studied experimentally. Those momentum profiles were obtained using the HEMS program outlined in Cook and Brion.[31] Note that those quantum chemical calculations were performed within the Gaussian 09 package.[32]

To investigate the dynamics of the electron impact ionization process, triple differential cross sections were calculated at the M3DW level. These calculations were performed for both the asymmetric coplanar and doubly symmetric coplanar scattering geometries. The triple differential cross section for electron-impact ionization can be obtained through

$$\frac{d\sigma}{d\Omega_a d\Omega_b dE_b} = \frac{1}{(2\pi)^5}\frac{k_1 k_2}{k_0} \times \left(|T_{dir}|^2 + |T_{exc}|^2 + |T_{dir} - T_{exc}|^2\right), \quad (2)$$

where T_{dir} is the direct ionization scattering amplitude described by

$$T_{dir} = \left\langle \chi_1^-(\boldsymbol{k}_1,\boldsymbol{r}_1)\, \chi_2^-(\boldsymbol{k}_2,\boldsymbol{r}_2)\, C_{scat-ejec}(\boldsymbol{r}_{12}) \times |V - U_0|\, \phi_{DY}^{OA}(\mathbf{r}_2)\, \chi_0^+(\boldsymbol{k}_0,\boldsymbol{r}_1)\right\rangle. \quad (3)$$

The exchange scattering amplitude, T_{exc}, is calculated in the same way as the direct scattering amplitude, except that the outgoing electrons in the final state are interchanged. In calculating scattering amplitudes, the initial state is the product of the incident distorted wave $\chi_0^+(\boldsymbol{k}_0,\boldsymbol{r}_1)$, and the orientation averaged Dyson orbital $\phi_{DY}^{OA}(\boldsymbol{r}_2)$. The final state is described as the product of distorted waves for the two outgoing electrons, $\chi_1^-(\boldsymbol{k}_1,\boldsymbol{r}_1)$ and $\chi_2^-(\boldsymbol{k}_2,\mathbf{r}_2)$, and a Coulomb distortion factor $C_{scat-ejec}(\boldsymbol{r}_{12})$. Here, $\boldsymbol{r}_{12}$ is the distance between the two outgoing electrons. If we neglect the Coulomb distortion factor in the final state, the M3DW reduces to the distorted-wave Born approximation (DWBA).

To calculate a TDCS employing a proper average, the fixed-in-space Dyson orbital replaces the orientation averaged Dyson orbital in the description of the initial state. The proper-averaged TDCS can then be obtained from the TDCS for fixed-in-space molecules by numerically performing a subsequent spherical averaging procedure.[14]

For furfural, the orientation-averaged or fixed-in-space Dyson orbitals are obtained using a frozen-orbital approximation. The Dyson orbital is then described by the ionized Kohn-Sham orbital (either 4a″ or 21a′) calculated within a density functional theory framework employing the standard hybrid B3LYP functional[30] with a TZ2P (triple-zeta with two polarization functions) Slater type basis set within the ADF 2007 (Amsterdam Density Functional) program.[33] More details about the M3DW method can be found in the work of Madison and Al-Hagan.[34]

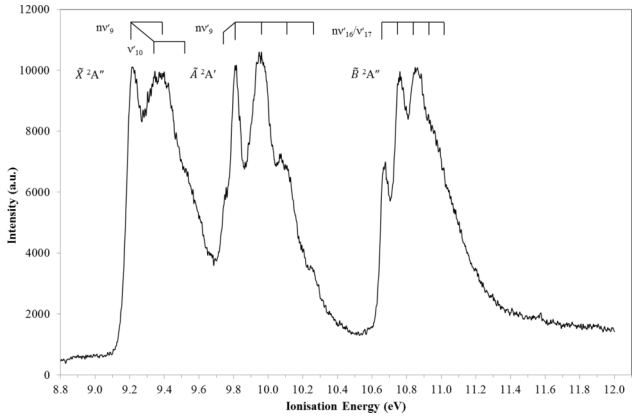

FIG. 3. The present He(I) photoelectron spectrum of furfural as measured in the 8.8–12.0 eV binding energy region.

In order to compare the calculated TDCS to the data, the TDCS were calculated for the HOMO and NHOMO of furfural in both the *cis* and *trans* conformers. A relative conformer population weighting 0.205 × (*cis*) and 0.795 × (*trans*) was then applied, which is in line with the known relative populations of the two conformers in the gas phase under the experimental conditions.[10,11] Owing to the high computational cost of performing the proper average calculations, these calculations were only performed for the NHOMO of the *trans* geometry which displayed a larger cross section at the M3DW level. As the proper average calculations are only performed for the NHOMO, we apply a normalisation factor to rescale this calculation so it can be compared with the experimental data and M3DW calculation. That normalisation factor was determined using a least squares fitting procedure

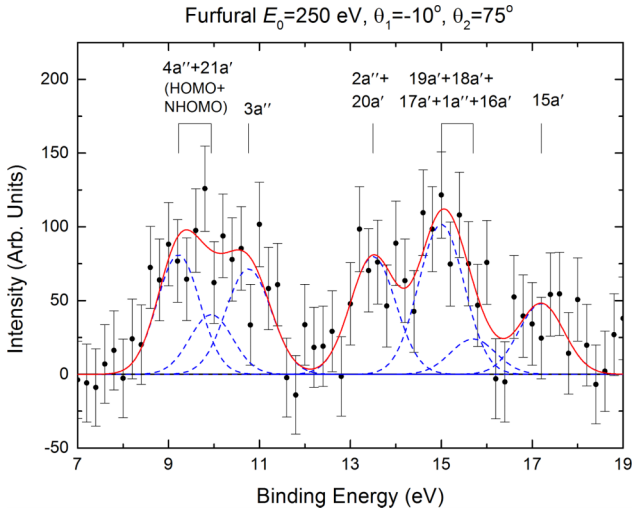

FIG. 4. A representative binding energy spectrum of furfural obtained in asymmetric coplanar kinematics with $E_0 = 250$ eV, $E_2 = 20$ eV, and the scattered and ejected electrons being detected at $\theta_1 = -10°$ and $\theta_2 = 75°$, respectively.

applied to the normalised experimental data of the binary region of the $\theta_1 = -10°$ angular distribution.

IV. RESULTS AND DISCUSSION

A. Photon and electron impact ionization and state assignments

In Figures 3 and 4, we present our high resolution photoelectron spectrum and the $(e,2e)$ binding energy spectrum obtained in the asymmetric coplanar geometry. In Table I, we further present a summary of the electronic state assignments, and where possible the assignments of the vibrational substructure for the ionic states of furfural. Those assignments are additionally compared to results from the calculations, and those made using the photoelectron spectrum previously reported by Klapstein and co-workers.[12] The high resolution photoelectron spectra display three distinct bands, peaking at 9.223 ± 0.002 eV ($4a''$, π), 9.956 ± 0.002 ($21a'$, n_O), and 10.678 ± 0.002 ($3a''$, π) eV. These values are largely consistent with the early photoelectron spectroscopic investigation.[12] The ionization processes of these three features either relate to the removal of electrons from the π-bonding structure of the 5-member ring, or to the oxygen lone-pair (n_O) in the carbonyl group. We do, however, note that in the $21a'$ orbital, the in-plane oxygen lone electron pair (n_O) does couple to the carbon frame through a σ–like interaction. The calculated values, shown in Table I, further suggest that both the *cis* and *trans* conformers all have

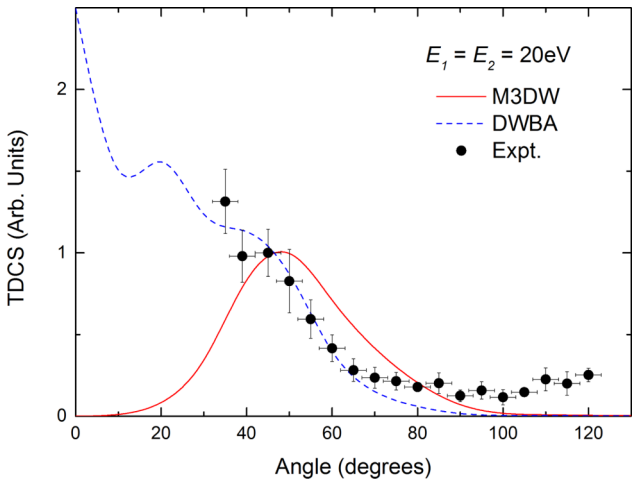

FIG. 5. Experimental and theoretical triple differential cross sections for electron impact ionization of the unresolved HOMO + NHOMO ($4a'' + 21a'$) of furfural in the double symmetric coplanar geometry. Here, the electrons were detected with $E_1 = E_2 = 20$ eV. See also legend in figure.

TABLE I. Experimental and theoretical ionization potentials (eV) of furfural. Also presented are the ionic vibrational state assignments and calculated pole strengths.

	Present PES						*cis*-furfural OVGF/aug-cc-pvdz		*trans*-furfural OVGF/aug-cc-pvdz	
Present $(e,2e)$	Energy (eV)	$\Delta\nu'$ (eV)	$\Delta\nu'$ (eV)	Assignment	PES[12]	State	Energy (eV)	PS	Energy (eV)	PS
9.2	9.223[a]	…	…	ν_{00}	9.22	$(4a'')^{-1}$	9.25	0.90	9.18	0.90
	9.346	0.123	…	$1\nu'_{10}$	9.32					
	9.382	…	0.159	$1\nu'_{9}$[b]	9.39					
	9.52(7)[c]	…	0.181	$1\nu'_{10}+1\nu'_{9}$[b]	9.57					
9.9	9.765	0.048	…	ν_{18}	…	$(21a')^{-1}$	10.46	0.88	10.49	0.88
	9.813[a]	…	…	ν_{00}	9.80[a]					
	9.956[d]	…	0.143	$1\nu'_{9}$	9.94[d]					
	10.07(4)[c]	…	0.118	$2\nu'_{9}$	10.08					
	10.24(8)[c]	…	0.174	$3\nu'_{9}$	10.22					
10.8	10.678	…	…	ν_{00}	10.67	$(3a'')^{-1}$	10.78	0.89	10.74	0.89
	10.765	0.087	…	$1\nu'_{16}/1\nu'_{17}$	10.76					
	10.860	0.095	…	$2\nu'_{16}/2\nu'_{17}$	10.86					
	10.92(9)[c]	0.069	…	$3\nu'_{16}/3\nu'_{17}$	10.96					
	11.02(6)[c]	0.097	…	$4\nu'_{16}/4\nu'_{17}$	…					
13.5					13.5	$(2a'')^{-1}$	13.76	0.83	13.79	0.83
						$(20a')^{-1}$	13.81	0.90	13.85	0.90
					14.3	$(19a')^{-1}$	14.57	0.90	14.52	0.90
15.0					14.8	$(18a')^{-1}$	14.72	0.89	14.68	0.89
15.7					15.97	$(17a')^{-1}$	15.74	0.87	15.30	0.88
						$(1a'')^{-1}$	15.77	0.76[e]	15.76	0.75[e]
						$(16a')^{-1}$	15.89	0.86	16.42	0.87
17.2					17.2	$(15a')^{-1}$	17.97	0.85	17.91	0.86

[a] Adiabatic value.
[b] See text for more detail.
[c] Shoulder structure (the last decimal of the energy value is given in brackets for these less-resolved features).
[d] Vertical value.
[e] Here the one-particle picture of ionization is breaking down.

very similar ionization energies. The measured low-lying vertical ionization energies of furfural in both conformations agree reasonably well, to within ±0.5 eV, with the OVGF theoretical predictions. Here, the OVGF theory is consistent with results from the density functional theory calculations at the B3LYP/aug-cc-pVDZ level, in that the ordering of the HOMO and NHOMO is 4a″ and 21a′, respectively.

The high-resolution photoelectron spectra also show substantially more detail for each of the initial three ionic bands than had been previously observed. The structures within each of these features are reminiscent of those observed in previous studies on furan,[35] its methyl derivative,[36] and 2-vinyl furan.[37] The first adiabatic energy of furfural is 9.223 ± 0.002 eV (Figure 3 and Table I), followed by a vibrational peak centred at 9.382 eV, which is 0.159 eV from the 0–0 transition. This peak is quite broad and asymmetric, and on the low energy side, a structure may be tentatively positioned at 0.123 eV from the origin. The weak broad band at higher energy [9.52(7) eV] may be mainly assigned to combination and overtone bands of these two vibrations. However, the relatively poorer apparent resolution here compared with the corresponding band in furan[35] and the other furan derivatives[36,37] suggests that many vibrations may be actively adding to the linewidth. This assignment of vibrational states is further complicated by the observation of Fermi resonances in the infrared vibrational excitation spectra.[38] We therefore tentatively propose the following possible vibrational mode assignments (with ground state vibration energies for *trans*- and *cis*-conformers, respectively): to the main 0.159 eV peak, ν_9 (0.169 eV) with other possible contributing vibrational modes ν_6 (0.195 and 0.194 eV), ν_7 (0.182 and 0.183 eV) and ν_8 (0.173 eV), and to the 0.123 eV feature, ν_{10} (0.155 and 0.158 eV). All these vibrations are totally symmetric (a′)[38] and involve displacement of the heavier atoms (C and O).[39] For the next ionic band, $\tilde{A}\ ^2A'$, the peak at 9.813 ± 0.002 eV is assigned to the 0–0 transition. The peak at 9.956 eV is therefore 0.143 eV from this origin. A possible contributing vibrational mode in this case is (with ground state vibration energies for *trans*- and *cis*-conformers, respectively) ν_9 (0.169 eV). A weak shoulder appears on the low energy side of the 0–0 transition, around 0.048 eV, and may be due to a hot-band involving mode ν_{18} (0.062 eV). As

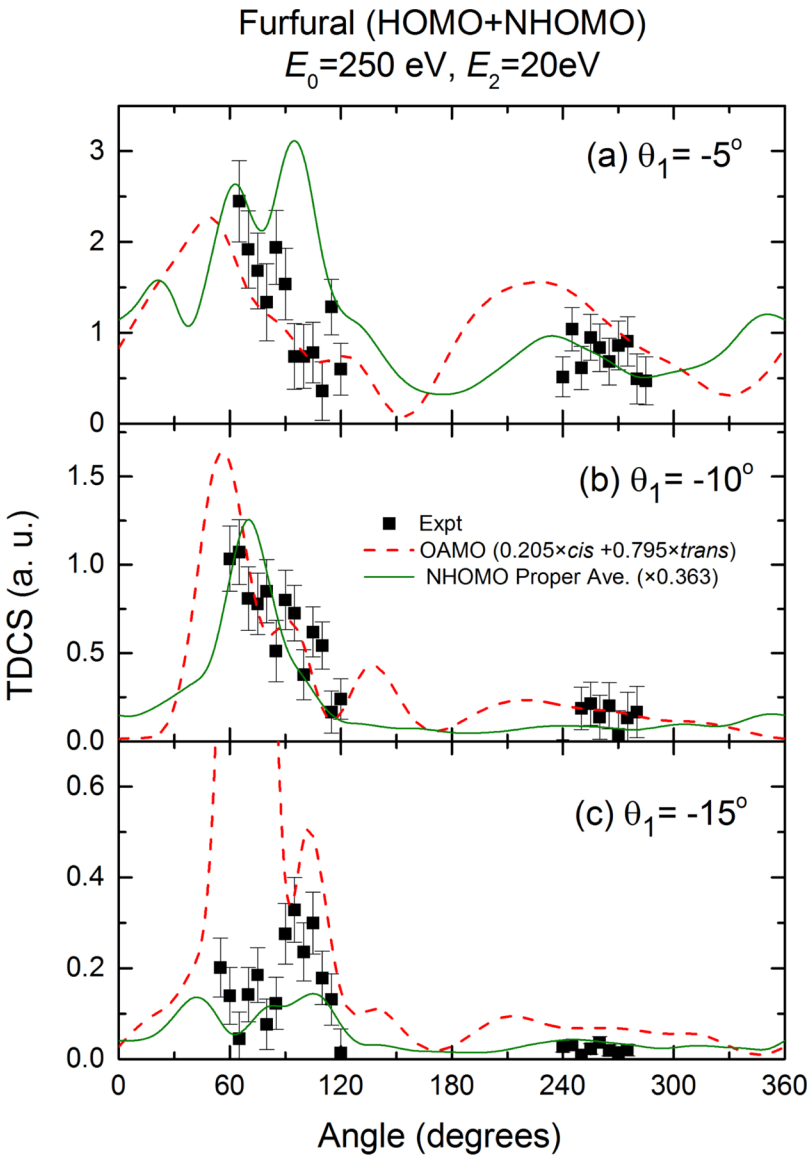

FIG. 6. Experimental and theoretical triple differential cross sections for electron impact ionization of the HOMO+NHOMO (4a″ + 21a′) of furfural in the asymmetric kinematics with $E_0 = 250$ eV, $E_2 = 20$ eV, and with the scattered electron being detected at (a) $\theta_1 = -5°$, (b) $\theta_1 = -10°$, and (c) $\theta_1 = -15°$. See text and legend in the figure for further details. Note that a.u. here represents atomic units.

far as the third ionic band is concerned, we assign the structure to either excitation of mode ν_{16} (0.109 eV) or ν_{17} (0.094 eV). As a consequence, we have labelled its features in Figure 3 and Table I as ν_{16}/ν_{17}.

B. Electron impact ionization dynamics

In Fig. 5, TDCS for the electron impact ionization of the unresolved HOMO+NHOMO ($4a'' + 21a'$) are presented, measured in the doubly symmetric coplanar geometry with a detected electron energy of 20 eV. The measured TDCSs are compared to theoretical calculations performed at the DWBA and the M3DW level. In order to facilitate a qualitative comparison between the experiment and different calculations, both the theoretical and experimental results have been normalised to unity at $\xi_1 = \xi_2 = \xi = 45°$ as noted above. In this comparison, it is observed that the DWBA calculation adequately reproduces the shape of the data in the 35°-65° range. However, the DWBA calculation gives unphysical behaviour in the limit of $\xi = 0°$, where the TDCS must be zero owing to the repulsive Coulombic interaction between the outgoing electrons. The M3DW calculation correctly accounts for this asymptotic behaviour; however, it fails to predict the correct shape of the experimental TDCS. Note that the TDCS data increase in intensity as the angle of detection increases from 100° to 120°. Interestingly, however, both the DWBA and M3DW calculations predict decreasing intensity as this angle increases.

TDCSs have also been measured in an asymmetric coplanar geometry, with the results presented in Fig. 6. Here, angular distributions of the ejected electrons ($E_2 = 20$ eV) were measured while the scattered electrons were detected at fixed angles of (a) $\theta_1 = -5°$, (b) $\theta_1 = -10°$, and (c) $\theta_1 = -15°$. The TDCSs are compared with corresponding results from M3DW calculations (for the HOMO+NHOMO) that either employ an orientation average molecular orbital (OAMO) or include a proper average to account for the random orientation of the target in the experiment. Here, we again note that as the experimental angular distributions for each scattered electron angle have been inter-normalised, only a single normalisation factor is employed between the M3DW calculation and the experimental data. We reiterate that this factor was determined using a least squares technique in the binary region of the $\theta_1 = -10°$ angular distribution.

In contrast to the doubly symmetric coplanar geometry, the M3DW calculations using an OAMO approach (dashed red

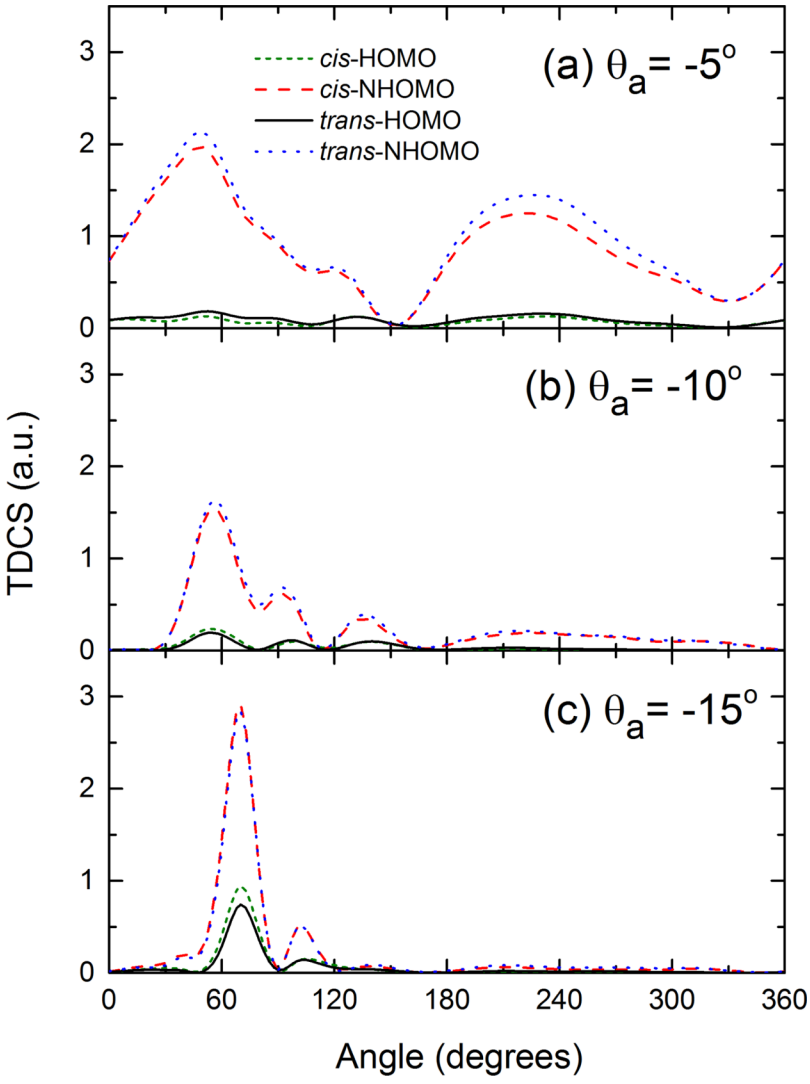

FIG. 7. Theoretical M3DW orientation averaged molecular orbital (OAMO) triple differential cross sections for electron impact ionization of the HOMO and NHOMO of each furfural conformer. Results are for asymmetric coplanar kinematics with $E_0 = 250$ eV, $E_2 = 20$ eV, and with the scattered electrons being detected at (a) $\theta_1 = -5°$, (b) $\theta_1 = -10°$, and (c) $\theta_1 = -15°$. Note that a.u. here represents atomic units. See also legend in figure.

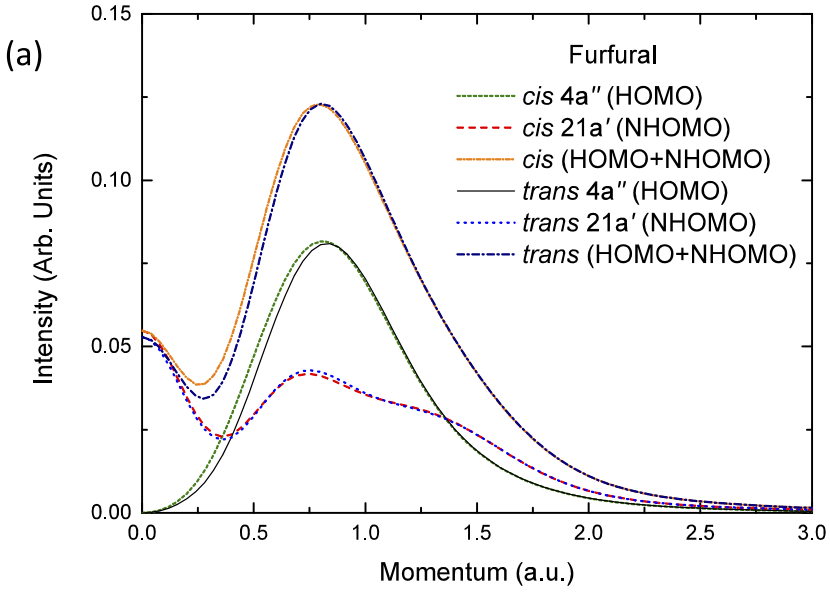

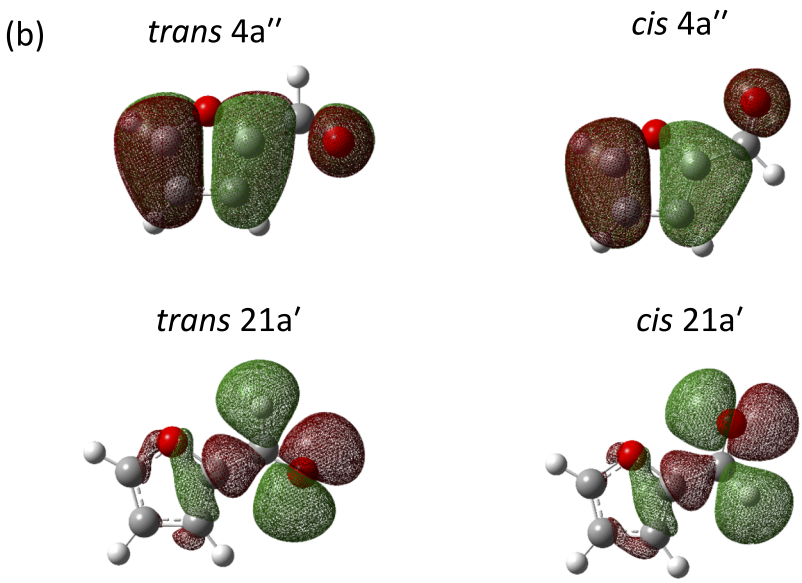

FIG. 8. (a) Theoretical spherically averaged momentum profiles and (b) molecular orbital representations of the HOMO and NHOMO of furfural in both the *cis* and *trans* conformers. See also legend in the figure.

line) qualitatively reproduce the shape and relative magnitude of the TDCS for the scattering angles of $\theta_1 = -5°$ and $-10°$ (see Fig. 6). However, the M3DW (OAMO) calculations fail to reproduce the experimental behaviour observed when the scattered electron angle is changed to $\theta_1 = -15°$. Specifically, the M3DW (OAMO) predicts that the TDCS has a maximum intensity in the direction of the momentum transfer, while experimentally a minimum is observed. The M3DW (OAMO) calculation also predicts a greater recoil intensity than that observed experimentally at $\theta_1 = -5°$ and $-15°$.

To try to understand these deficiencies in the M3DW (OAMO) model, calculations employing a proper TDCS average were also performed. These calculations are computationally demanding, so they were restricted to electron-impact ionization of the NHOMO. This restriction, being different from that which is measured in the experiments, led us to normalise those proper average calculations to the experimental data. It is hoped that these computationally demanding calculations for the NHOMO will still provide some insights into the merits of the proper TDCS averaging procedure in general. These results are represented by the solid green lines in Fig. 6.

The proper average result has more success in resolving the observed discrepancies in the angular distribution of the binary region for a scattered electron angle of $\theta_1 = -15°$. Further, the proper average result displays relative binary and recoil peak intensities that are somewhat consistent with those observed experimentally. This suggests that the proper average might resolve the deficiencies within the OAMO approach. However, the significant computational cost, thus only allowing for the calculation of the proper average TDCS for the NHOMO, while experimentally the HOMO and NHOMO are investigated, does limit our ability to fully assess the merits of this theoretical approach.

It is therefore important to try to understand the sources of the discrepancies observed between experiment and theory

at the M3DW (OAMO) level, particularly given this high computational cost of carrying out the proper average calculations. To assist in this, TDCS obtained at the M3DW level (with an orbital average) for the HOMO and NHOMO of both conformers are presented in Fig. 7. Additionally, in Fig. 8 we present orbital momentum profiles and schematic diagrams of the ionized orbitals. In Fig. 7, it is seen that the TDCS calculated for the NHOMO is substantially larger in magnitude than that for the HOMO, for almost the entire angular distribution of each scattered electron angle considered. When the spherically averaged momentum profiles for the HOMO and NHOMO are considered in Fig. 8, it is only in the smallest ($\lesssim$0.3 a.u.) or largest ($\gtrsim$1.3 a.u.) momentum regions that the NHOMO displays larger intensity than that for the HOMO. Note that in high-impact energy electron impact ionization kinematics where the collision can be described impulsively, the TDCS is proportional to the modulus squared of the spherically averaged orbital momentum profile (i.e., so called electron momentum spectroscopy[25,40]). While the present asymmetric coplanar kinematical conditions substantially differ from those required to probe the orbital structure, we have previously observed that the underlying orbital character still persists in the angular distribution of the dynamical TDCS under similar conditions.[16–20] Here, we note that the influence of an orbital's character to TDCS behaviour was first discussed in Xu *et al.*[41] In this study, the range of recoil momenta magnitudes covered in these asymmetrical kinematics are 0.77-1.66 a.u., 0.44-1.98 a.u., and 0.10-2.33 a.u for $\theta_1 = -5°$, $-10°$, and $-15°$, respectively. For this reason, it appears that the calculations for the TDCS of the M3DW (OAMO) HOMO may be substantially underestimated. Note also that the M3DW failed to describe the observed angular distribution for the HOMO+NHOMO of phenol.[19] In the case of phenol, both the HOMO and NHOMO are dominated by orbital contributions that form an out-of-plane π-bonding network. This is similar to the HOMO of furfural, which can also be described as an out-of-plane π-bonding orbital. We therefore suspect that the inverse symmetry, or a substantial delocalisation of these orbital contributions away from the nucleons, is the cause of the reduction in the TDCS intensity of the HOMO within the orbital average M3DW framework. This therefore represents a limitation in the application of that theoretical approach.

V. CONCLUSIONS

In this manuscript, an in-depth study into the photon and electron impact ionization to low-lying ionic states of furfural has been presented. Measurement of high resolution He(I) photoelectron spectra has provided the first vibrational spectral assignments of the ionic states. The dynamics of the electron-impact ionization process have been evaluated in asymmetric coplanar and doubly symmetric coplanar geometries. These results have been compared to those from sophisticated molecular three-body distorted wave calculations that employ either an orbital or proper average to account for the random orientation of the target. It was observed that in asymmetric kinematics, the orientation average failed to accurately reproduce the angular dependence of the measurements over the complete set of kinematical conditions studied experimentally. The inter-normalisation of the experimental TDCS measurements for different scattered angles also revealed discrepancies with the absolute scale of the M3DW calculations within the orbital average formulation. TDCSs calculated using a proper average appear to resolve some of these problems, however, their high computational cost makes them prohibitive for calculating all possible contributing states (the results presented here took over one year to calculate using all of the available computing resources at our disposal). It therefore remains desirable to understand the limitations within the orientation average M3DW model. Clearly, strategies for reducing the computational demands of the proper average calculations are desirable so that the merits of this approach can be definitively assessed.

ACKNOWLEDGMENTS

P.L.V. acknowledges the Portuguese Foundation for Science and Technology (FCT-MEC) through research Grant Nos. PTDC/FIS-ATO/1832/2012, SFRH/BSAB/105792/2014, and UID/FIS/00068/2013. He also acknowledges his Visiting Professor position at Flinders University and together with M.-J.H.-F., the Portuguese–Belgian joint collaboration. The Patrimoine of the University of Liège, the Fonds National de la Recherche Scientifique, and the Fonds de la Recherche Fondamentale Collective of Belgium have supported this research. D.B.J. thanks the Australian Research Council for financial support provided through a Discovery Early Career Research Award, while M.J.B. also thanks the Australian Research Council for financial support. E.A. and D.H.M. acknowledge support of the U.S. National Science Foundation (NSF) under Grant No. PHY-1068237 and XSEDE resources provided by the Texas Advanced Computing Center (Grant No. TG-MCA07S029). Computational work was performed with Institutional Computing resources made available through the Los Alamos National Laboratory. The Los Alamos National Laboratory is operated by Los Alamos National Security, LLC, for the National Nuclear Security Administration of the U.S. Department of Energy under Contract No. DE-AC5206NA25396. C.G.N. acknowledges support of the National Natural Science Foundation of China (NNSFC) under Grant No. 11174175. K.L.N. would like to thank CNPq for an "Attracting Young Talent" grant and also thanks the Royal Society for funding her visit to the University of Manchester as a Newton Alumni. We all thank Rafael Neves for some assistance in operating the spectrometer at Flinders.

[1]A. S. Mamman, J.-M. Lee, Y.-C. Kim, I. T. Hwang, N.-J. Park, Y. K. Hwang, J.-S. Chang, and J.-S. Hwang, Biofuels, Bioprod. Biorefin. **2**, 438 (2008).
[2]H. Gomez Bernal, L. Bernazzani, and A. M. Raspolli Galletti, Green Chem. **16**, 3734 (2014).
[3]J.-P. Lange, E. van der Heide, J. van Buijtenen, and R. Price, ChemSusChem **5**, 150 (2012).
[4]A. J. Ragauskas, C. K. Williams, B. H. Davison, G. Britovsek, J. Cairney, C. A. Eckert, W. J. Frederick, J. P. Hallett, D. J. Leak, C. L. Liotta, J. R. Mielenz, R. Murphy, R. Templer, and T. Tschaplinski, Science **311**, 484 (2006).
[5]J. Amorim, C. Oliveira, J. A. Souza-Corrêa, and M. A. Ridenti, Plasma Processes Polym. **10**, 670 (2013).
[6]N. Schultz-Jensen, F. Leipold, H. Bindslev, and A. Thomsen, Appl. Biochem. Biotechnol. **163**, 558 (2011).

[7]J. S. Bak, J. K. Ko, Y. H. Han, B. C. Lee, I.-G. Choi, and K. H. Kim, Bioresour. Technol. **100**, 1285 (2009).
[8]A. W. Khan, J. P. Labrie, and J. McKeown, Biotechnol. Bioeng. **28**, 1449 (1986).
[9]V. A. Igor and R. L. Walter, Plasma Phys. Controlled Fusion **57**, 014001 (2015).
[10]K. K. Baldridge, V. Jonas, and A. D. Bain, J. Chem. Phys. **113**, 7519 (2000).
[11]T. S. Little, J. Qiu, and J. R. Durig, Spectrochim. Acta, Part A **45**, 789 (1989).
[12]D. Klapstein, C. D. MacPherson, and R. T. O'Brien, Can. J. Chem. **68**, 747 (1990).
[13]F. Ferreira da Silva, E. Lange, P. Limão-Vieira, N. C. Jones, S. V. Hoffmann, M.-J. Hubin-Franskin, J. Delwiche, M. J. Brunger, R. F. C. Neves, M. C. A. Lopes, E. M. de Oliveira, R. F. da Costa, M. T. do N. Varella, M. H. F. Bettega, F. Blanco, G. García, M. A. P. Lima, and D. B. Jones, J. Chem. Phys. **143**, 144308 (2015).
[14]H. Chaluvadi, C. G. Ning, and D. Madison, Phys. Rev. A **89**, 062712 (2014).
[15]S. M. Bellm, J. D. Builth-Williams, D. B. Jones, H. Chaluvadi, D. H. Madison, C. G. Ning, F. Wang, X. G. Ma, B. Lohmann, and M. J. Brunger, J. Chem. Phys. **136**, 244301 (2012).
[16]J. Builth-Williams, S. M. Bellm, D. B. Jones, H. Chaluvadi, D. Madison, C. G. Ning, B. Lohmann, and M. J. Brunger, J. Chem. Phys. **136**, 024304 (2012).
[17]J. D. Builth-Williams, S. M. Bellm, L. Chiari, P. A. Thorn, D. B. Jones, H. Chaluvadi, D. H. Madison, C. G. Ning, B. Lohmann, G. B. da Silva, and M. J. Brunger, J. Chem. Phys. **139**, 034306 (2013).
[18]D. B. Jones, J. D. Builth-Williams, S. M. Bellm, L. Chiari, H. Chaluvadi, D. H. Madison, C. G. Ning, B. Lohmann, O. Ingolfsson, and M. J. Brunger, Chem. Phys. Lett. **572**, 32 (2013).
[19]G. B. da Silva, R. F. C. Neves, L. Chiari, D. B. Jones, E. Ali, D. H. Madison, C. G. Ning, K. L. Nixon, M. C. A. Lopes, and M. J. Brunger, J. Chem. Phys. **141**, 124307 (2014).
[20]J. D. Builth-Williams, G. B. da Silva, L. Chiari, D. B. Jones, H. Chaluvadi, D. H. Madison, and M. J. Brunger, J. Chem. Phys. **140**, 214312 (2014).
[21]J. Delwiche, P. Natalis, J. Momigny, and J. E. Collin, J. Electron Spectrosc. Relat. Phenom. **1**, 219 (1972).
[22]J. H. D. Eland, *Photoelectron Spectroscopy* (Butterworth & Co., Ltd., London, 1984).
[23]*Handbook of Chemistry and Physics*, edited by D. R. Lide (CRC Press, New York, 1992).
[24]S. J. Cavanagh and B. Lohmann, J. Phys. B: At., Mol. Opt. Phys. **32**, L261 (1999).
[25]E. Weigold and I. E. McCarthy, *Electron Momentum Spectroscopy* (Kluwer Academic/Plenum Publishers, New York, 1999).
[26]A. J. Murray, B. C. H. Turton, and F. H. Read, Rev. Sci. Instrum. **63**, 3346 (1992).
[27]W. von Niessen, J. Schirmer, and L. S. Cederbaum, Comput. Phys. Rep. **1**, 57 (1984).
[28]T. H. Dunning, J. Chem. Phys. **90**, 1007 (1989).
[29]R. A. Kendall, T. H. Dunning, and R. J. Harrison, J. Chem. Phys. **96**, 6796 (1992).
[30]C. Lee, W. Yang, and R. G. Parr, Phys. Rev. B **37**, 785 (1988).
[31]J. P. D. Cook and C. E. Brion, Chem. Phys. **69**, 339 (1982).
[32]M. J. Frisch *et al.*, GAUSSIAN 09, Revision B.01, Gaussian, Inc., Wallington, CT, 2010.
[33]G. te Velde, F. M. Bickelhaupt, E. J. Baerends, C. Fonseca Guerra, S. J. A. van Gisbergen, J. G. Snijders, and T. Ziegler, J. Comput. Chem. **22**, 931 (2001).
[34]D. H. Madison and O. Al-Hagan, J. At., Mol., Opt. Phys. **2010**, 367180.
[35]E. E. Rennie, C. A. F. Johnson, J. E. Parker, D. M. P. Holland, D. A. Shaw, M. A. MacDonald, M. A. Hayes, and L. G. Shpinkova, Chem. Phys. **236**, 365 (1998).
[36]A. Giuliani, J. Delwiche, S. V. Hoffmann, P. Limão-Vieira, N. J. Mason, and M.-J. Hubin-Franskin, J. Chem. Phys. **119**, 3670 (2003).
[37]A. Giuliani, I. C. Walker, J. Delwiche, S. V. Hoffmann, C. Kech, P. Limão-Vieira, N. J. Mason, and M.-J. Hubin-Franskin, J. Chem. Phys. **120**, 10972 (2004).
[38]M. Rogojerov, G. Keresztury, and B. Jordanov, Spectrochim. Acta, Part A **61**, 1661 (2005).
[39]T. Kim, R. S. Assary, L. A. Curtiss, C. L. Marshall, and P. C. Stair, J. Raman Spectrosc. **42**, 2069 (2011).
[40]M. Takahashi, Bull. Chem. Soc. Jpn. **82**, 751 (2009).
[41]S. Xu, X. Ma, S. Yan, and P. Zhang, J. Chem. Phys. **136**, 237101 (2012).